Mon. Not. R. Astron. Soc. **000**, 000–000 (0000) Printed 19 April 2007 (MN LATEX style file v2.2)

A Submillimetre Imaging Polarimeter at the James Clerk Maxwell Telescope

J.S. Greaves[1,2], W.S. Holland[1,2], T. Jenness[1], A. Chrysostomou[3,1], D.S. Berry[4,5], A.G. Murray[6,8], M. Tamura[9], E.I. Robson[1,5] P.A.R. Ade[6,7], R. Nartallo[6,7], J.A. Stevens[10,2], M. Momose[11], J.-I. Morino[12], G. Moriarty-Schieven[13,1], F. Gannaway[6,7], C.V. Haynes[6,7]

[1]*Joint Astronomy Centre, 660 N. A'oh¯ok¯u Place, UniversityPark, Hilo, Hawaii 96720, USA*
[2]*UK Astronomy Technology Centre, Royal Observatory, Blackford Hill, Edinburgh EH9 3HJ, UK*
[3]*Division of Physical Sciences, University of Hertfordshire, College Lane, Hatfield, Herts. AL10 9AB, UK*
[4]*Department of Physics and Astronomy, University of Manchester, Manchester, M13 9PL, U.K*
[5]*Centre for Astrophysics, University of Central Lancashire, Preston, Lancs. PR1 2HE, UK*
[6]*Department of Physics, Queen Mary, University of London, Mile End Rd., London E1 4NS, UK*
[7]*Department of Physics and Astronomy, Cardiff University, P.O. Box 913, Cardiff CF2 3YB, Wales*
[8]*Moray College, Moray St., Elgin IV30 1JJ, UK*
[9]*National Astronomical Observatory of Japan, Osawa, Mitaka, Tokyo 181-8588, Japan*
[10] *Mullard Space Science Laboratory, University College London, Holmbury St. Mary, Dorking, Surrey, RH5 6NT*
[11]*Institute of Astrophysics and Planetary Sciences, Ibaraki University, Bunkyo 2-1-1, Mito, Ibaraki 310-8512, Japan*
[12]*Subaru Telescope, 650 N. A'oh¯ok¯u Place, Hilo, HI 96720, USA*
[13]*National Research Council of Canada, Herzberg Institute of Astrophysics, 5071 West Saanich Road, Victoria, BC, V9E 2E7, Canada*

arXiv:astro-ph/0302609v1 28 Feb 2003

19 April 2007

ABSTRACT

A polarimeter has been built for use with the Submillimetre Common-User Bolometer Array (SCUBA), on the James Clerk Maxwell Telescope (JCMT) in Hawaii. SCUBA is the first of a new generation of highly sensitive submillimetre cameras, and the UK/Japan Polarimeter adds a polarimetric imaging/photometry capability in the wavelength range 350 to 2000 μm. Early science results range from measuring the synchrotron polarization of the black hole candidate Sgr A* to mapping magnetic fields inferred from polarized dust emission in Galactic star-forming clouds. We describe the instrument design, performance, observing techniques and data reduction processes, along with an assessment of the current and future scientific capability.

Key words:
instrumentation: polarimeters — techniques: polarimetric — submillimetre — polarization — magnetic fields

1 INTRODUCTION

Linear polarization of submillimetre continuum radiation is associated with optically-thin synchrotron emission, and with partial magnetic alignment of elongated dust grains. In both cases, magnetic morphology can be deduced from the directions of polarization vectors, and these techniques are much less subject to confusion than in the optical and radio regimes, where scattering and Faraday rotation dominate the polarized signal. In the submillimetre, the limitations are that the data are only sensitive to the net plane-of-the-sky magnetic field direction within the telescope beam, and that there is no direct information on magnetic field strengths. However, with the capability to detect levels of linear polarization of 1% or less, considerable magnetic *structure* information can be obtained. The importance of magnetic fields is now being realised in sources ranging from disks around young stellar objects to the inner jets in active galactic nuclei (Tamura et al. 1999; Nartallo et al. 1998).

Observing techniques at submillimetre wavelengths have matured considerably in the last decade, particularly with the introduction of the first generation of continuum cameras. The chief difficulty for ground-based observations is the high opacity and time variability of the Earth's atmosphere, and these problems are critical for polarimetry. Atmospheric absorption can be largely overcome by building telescopes at suitable high, dry sites, such as

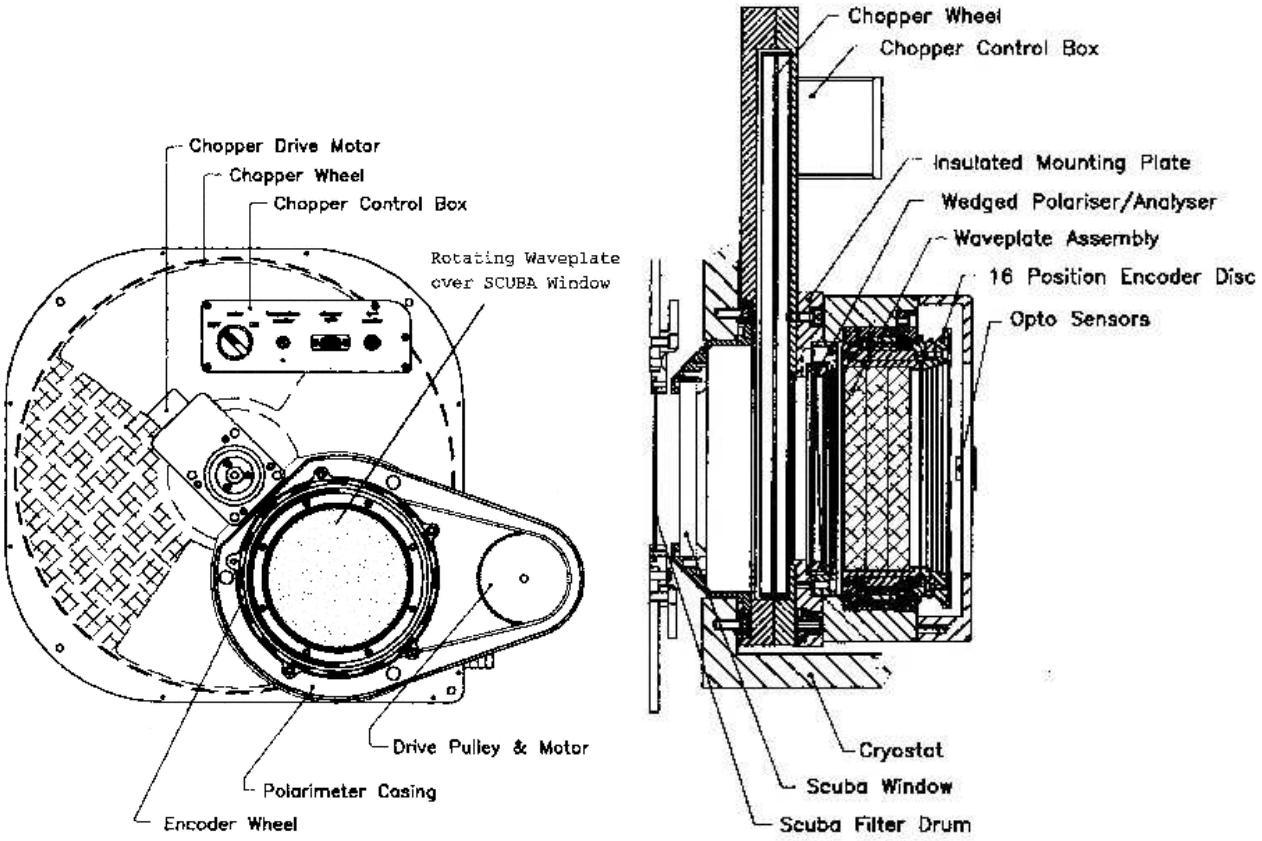

Figure 1. Technical drawing of polarimeter (from Murray et al. (1997)). The physical dimensions of the polarimeter module are 30 by 10 cm (maximum length and thickness respectively). The waveplates are 12 cm in diameter; the thickness of individual half-wave quartz plates depends on wavelength but a representative value is 0.9 cm for a single plate optimised for 850 μm observations and made of quartz with a submillimetre refractive index of 2.1.

Mauna Kea in Hawaii (summit altitude 4200m), and by observing in frequency 'windows' away from oxygen and water absorption lines. Under the best conditions, the zenith transmission is then about 80% at a wavelength of 850 μm, and as much as 40% at shorter wavelengths such as 450 μm. The other problem affecting the quality of flux measurements is atmospheric instability, especially emissivity changes on short timescales of a few seconds. This is a particular challenge for polarimetric observations, which require measurements accurate to better than 1% over periods of minutes to hours, and necessitates sophisticated techniques for removing sky-level changes.

Submillimetre polarimetry using single-pixel photometers began about a decade ago (e.g., Flett & Murray 1991), and a number of important detections were made both in the (sub)millimetre (e.g., Kane et al. 1993; Greaves et al. 1997; Glenn et al. 1999) and with complementary studies of warmer sources in the far-infrared (e.g., Novak et al. 1989). These observations were extremely laborious, but a major breakthrough has been made with the arrival of sensitive submillimetre and far-infrared cameras. With the inclusion of polarimeters — typically based on rotating half-wave plate designs and either internal or external to the cryogenically cooled instrument — polarization imaging of a wide variety of sources has now become feasible. A complete introduction has been presented by Hildebrand et al. (2000). In this paper, we describe observations and techniques with the new imaging polarimeter[1] used with SCUBA, the Submillimetre Common-User Bolometer Array (Holland et al. 1999) at the James Clerk Maxwell Telescope (JCMT) on Mauna Kea.

2 INSTRUMENT DESIGN AND PERFORMANCE

The general design of the polarimeter has been described by Murray et al. (1997). It is an external module that fits over the SCUBA cryostat window, and comprises a rotating half-waveplate and a fixed photo-lithographic grid ('analyser') (Figure 1). The waveplate is stepped to a series of fixed angles, which has the effect of rotating the incoming source plane of polarization, by twice the physical angle of rotation. The grid, with a 10 micron line spacing (of etched copper on a mylar substrate), efficiently reflects one plane of polarization that is fixed in the SCUBA reference frame. The net effect (Figure 2) is to select out a fixed component of a rotated linearly polarized signal, so that the SCUBA bolometers see a modulated signal of the form

$$S(\delta) = 1/2[I_u + I_p(1 + cos(4\delta - 2\theta))]. \quad (1)$$

[1] The SCUBA Polarimeter has been funded jointly by the UK Particle Physics and Astronomy Research Council and the NAOJ and JSPS of Japan. SCUBA was funded by the JCMT Development Fund supported by PPARC, the National Research Council of Canada and the Netherlands Organisation for Pure Research, and built by the Royal Observatory Edinburgh, now the UK Astronomy Technology Centre.

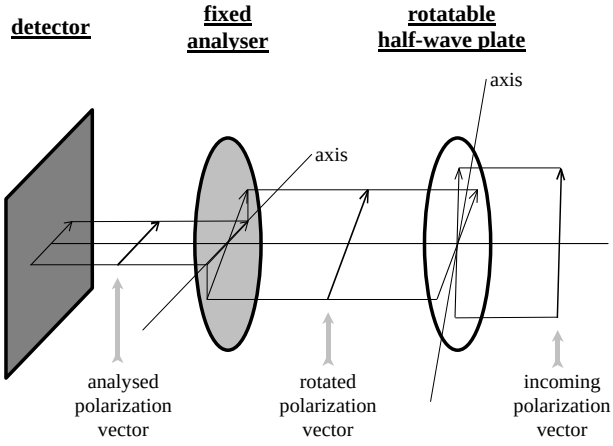

Figure 2. Illustration of the effects of a rotating half-waveplate and analyser (Berry & Gledhill 2000).

Here I_u is the unpolarized intensity, I_p describes the modulating polarized component above the minumum observed signal I_u, δ is the waveplate angle, and θ is the position angle of the polarization in a suitable co-ordinate frame. The factor of $1/2$ arises because one plane of polarization is reflected by the analyser; this contrasts with cameras designed specifically for polarimetry, which typically use a waveplate inside the instrument and measure both planes of polarization using two separate detector arrays (Dowell et al. 1998).

2.1 Waveplate design

The waveplates are made of birefringent quartz, cut to a thickness to retard one plane of polarization by half a wavelength relative to the orthogonal plane, on emerging from the plate. Since SCUBA has filters for observing at a wide range of wavelengths, from 0.35 to 2 mm, an *achromatic* design was adopted following the Pancharatnam method (Murray et al. 1997; Title & Rosenberg 1981). This uses a sandwich of an odd number of individual half-waveplates whose 'fast' axes of polarization are offset by $\pm 60^\circ$. The effect is a combined plate whose fast-axis direction (ϕ) is slightly wavelength-dependent, but with very good polarization modulation efficiency (PME) over a broad range of wavelengths. The plates were wax-bonded and then held in place in mounting rings. A good transmission (η) was achieved using single-layer polypropylene coatings to reduce reflections at the plate surfaces.

For the SCUBA polarimeter, two achromatic designs were used: one with three quartz plates to cover the 1.1, 1.35 and 2 mm bands and one with five plates for the 350, 450, 750 and 850 μm bands. Because SCUBA has single photometers at the millimetre wavelengths and full imaging arrays at the submillimetre wavelengths, the plates are known as 'photometric' and 'array' for convenience.

2.2 Performance on the JCMT

The performance of the waveplates on the telescope was first measured in October 1997, and the results are given in Table 1. Excellent PME values were measured, close to 100% at all wavelengths, and it was even found possible to operate the photometry plate in second order ($3\lambda/2$) at the array wavelengths. (This has advantages for complex observing programmes, because the polarimeter need not be removed to change the plate.) Nominally, measured polarization percentages should be divided by the PME to obtain the true values, but in practice this small correction is usually neglected. The transmission properties met the specifications for a single-layer coating, except at the shortest observing wavelengths, and it is suspected that re-coating and bonding of the plate might be necessary to improve this.

Table 1. Waveplate properties (symbols defined in the text). The input signal was produced with a second analyser to make a pure linear polarization from an astronomical source (generally Saturn). The PME is a function of waveplate angle with respect to the incoming plane, but minimum and mean values differ by no more than 8%. The ϕ values in brackets refer to observations after late 1998, when the photometric plate was re-mounted; the 1350 μm value was measured and the shift at 2000 μm was inferred.

λ (μm)	mean PME (%)	ϕ (degrees)	η (%)
'Array' waveplate			
350	96	+9	—
450	97	+7	∼60%
750	99	+1	—
850	97	–5	>85%
'Photometric' waveplate			
450	95	+7	—
850	94	+6	—
1350	99	+18 (+8)	>85%
2000	93	+3 (–7)	>85%

2.3 Reproducibility

An important part of the commissioning test was to confirm that the results agreed with previous polarimetric observations, from the JCMT and elsewhere. Tests included both low and high polarization sources: for example,

- 850 μm polarization of the DR21 cloud core was measured to be $1.70 \pm 0.27\%$ at $22 \pm 4^\circ$, whereas Minchin & Murray (1994) found $1.8 \pm 0.3\%$ at $17 \pm 4^\circ$ at 800 μm
- a flux peak in the Crab Nebula was detected at 1350 μm with $25.9 \pm 0.6\%$ polarization at $148 \pm 1^\circ$, while Flett & Murray (1991) obtained $25 \pm 2\%$ at $144 \pm 2^\circ$ at 1100 μm.

These results were from previous photometric polarimetry at the JCMT, and are for dust and synchrotron emission respectively. Since the previous instrument had no imaging capability, reproducibility in this mode relied on data from other telescopes: for example, our 850 μm polarization map of OMC1 (Coppin et al. 2000) is very similar to the 350 μm results of Schleuning (1998, his Figure 5). The position angles of dust polarization should be wavelength-independent provided that the telescope beams sample the same grain population and line-of-sight (Hildebrand et al. 2000).

2.4 Sensitivity limits

The sensitivity for polarization measurements is determined essentially by the sensitivity of SCUBA, with additional effects of the transmission through the polarimeter and the limiting accuracy of corrections for sky fluctuations. The critical quantity is the polarized flux: the product of percentage polarization and mean flux. With the previous JCMT polarimeter used on a single-bolometer

Table 2. Percentage and position angle (p, θ) of the main-beam instrumental polarization (not corrected for PME or ϕ); for the array data the uncertainties are the standard error of the set of individual measurements. Observations were made using several planets; note that Saturn may be slightly polarized due to scattering by the rings (with an best-fit value of 0.5% at 850 μm); however this effect is greatly reduced in data averaged over many hour angles. Saturn is also larger than the beam size at all the submillimetre wavelengths, so these data include some degree of sidelobe polarization.

λ (μm)	p(IP) (%)	θ_0(IP) (degrees)	source	epoch
Array waveplate (central array bolometer)				
350	0.82 ± 0.13	100 ± 4	Saturn	Oct 1997 + Aug 1999
450	3.51 ± 0.34	113 ± 3	Mars/Uranus	1997–1999 (5 dates)
750	1.16 ± 0.04	97 ± 1	Saturn	Oct 1997 + Aug 1999
850	1.09 ± 0.06	161 ± 2	Mars/Uranus	1997–1999 (25 dates)
Array waveplate (off-centre bolometers)				
450	3.26 ± 0.23	100 ± 2	Saturn	Jul 1998 (6 bolometers only)
850	0.92 ± 0.05	163 ± 2	Mars/Uranus/Saturn	1997–1999 (4 dates, all 36 bolometers)
Photometric waveplate				
1350	1.72 ± 0.11	166 ± 2	Uranus	1997–1999 (7 dates)
2000	1.34 ± 0.09	170 ± 1	Saturn/Uranus	Oct 1997 & Aug 1999

detector, UKT14, the smallest polarized flux that could be measured was about 100 mJy at 800 μm (Murray et al. 1997). This is equivalent, for example, to p = 1% in a 10 Jy source, such as one of the brightest Galactic protostars.

With the SCUBA polarimeter, the expected sensitivity can be derived by considering the magnitude of the fractional polarization, as obtained by subtracting signals at two waveplate angles and dividing by their sum[2]. The error on the polarization fraction is $1/\sqrt{2}$ times the fractional intensity error, so half as much time is needed as would be for a measurement of I alone. However, this is cancelled by a factor of twice as much time that arises because half the photons are lost to reflection off the analyser. Finally there is another time factor of four because four waveplate positions are needed to obtain the two orthogonal linear polarization components (Stokes parameters). This determines the signal-to-noise on the polarization percentage, σ_p, for a given integration time t:

$$t = 4/\eta \times N \times (\mathrm{NEFD}\sigma_p/pF)^2 \quad (2)$$

where NEFD and F are the noise equivalent flux density and source flux in mJy/$\sqrt{\mathrm{Hz}}$ and mJy respectively, and p is the fractional polarization (e.g. 0.01 for 1%). The factor N is the inverse of the fraction of time spent on one spatial point, so it is 1 for photometric polarimetry, 4 for imaging polarimetry at beam width spacings, and 16 for a Nyquist-sampled polarization map.[3]

At the primary observing wavelength of 850 μm, the NEFD is 70 mJy/$\sqrt{\mathrm{Hz}}$ under the best conditions, and a 1 hour integration would give a 3σ detection for a polarized flux $p \times F = 15$ mJy in a beam-spaced map, or 7.5 mJy for photometry. This signal-to-noise is sufficient to determine magnetic field directions to 0.5 radians / 3 (Naghizadeh-Khouei & Clarke 1993), or about $\pm 10^\circ$, and the sensitivity is more than an order of magnitude better than with the UKT14 polarimeter. The faintest sources actually detected have had fluxes of about 0.2 Jy per beam and polarizations of a few percent; scientifically, large samples of protostars, faint Galactic clouds and AGN can now be detected. Also, types of sources that were previously impossible can now be studied, including asteroids, prestellar cores and nearby starburst galaxies.

3 INSTRUMENTAL LIMITATIONS

3.1 Main-beam instrumental polarization

The absolute accuracy of any polarization measurement depends on how reliably instrumental effects can be subtracted. For the SCUBA polarimeter the main problem is instrumental polarization (IP), which is dominated by the woven Goretex windblind through which the JCMT observes. The thread spacing, which is approximately 0.5 mm, is slightly different in the vertical and horizontal directions and this affects the relative transmissions, particularly at a wavelength of 450 μm which is closest in size. The solution would be to either roll back the windblind (a half-hour labour-intensive operation that is only possible on rare occasions of very low windspeed) or add a second orthogonal sheet of Goretex in the beam to induce IP cancellation. The latter has been tried and reduced the IP by a factor of at least three at 450 μm; further experiments are ongoing but this is not yet the standard observing mode.

The IP in the main beam of the telescope has been measured using planets, assumed to be unpolarized (e.g., Clemens et al. 1990), and the results are listed in Table 2. At the primary wavelength of 850 μm the measured IP values are very stable and can be subtracted to an accuracy of about ± 0.25%, the measurement uncertainty for individual bolometers. Global differences, such as off-axis effects in the three rings of bolometers that form the hexagonal close-packed array, are 0.1% or less, and for the central array bolometer (used for photometric polarimetry) the measurement error has been reduced to about ± 0.06%. Fewer data are available at other wavelengths but generally a very accurate measurement can be made during a particular observing run. Values tend to be stable over time, taking into account that the angles must be corrected for telescope elevation. The observed θ is θ_0 plus elevation, due to

[2] Two waveplate angles 45° apart will have the largest and smallest observed signals, I_{max} and I_{min}, and it can be demonstrated from Equation 1 that $(I_{max} - I_{min})/(I_{max} + I_{min})$ is equivalent to the polarization fraction, $p = I_p/(I_u + I_p)$. For convenience we re-write $p = (R-1)/(R+1)$ where $R = I_{max}/I_{min}$, and differentiate this to give $dp = 2/(R+1)^2 dR$. For small polarizations $R \approx 1$ so $dp \approx dR/2$. Then as the two I measurements are independent, $dR/R = \sqrt{2} dI/I$ and combining the last two expressions, $dp = dI/I \times 1/\sqrt{2}$ in the limit $R \to 1$.

[3] The SCUBA beams are spaced two beam widths apart on the sky, so that at beam width resolution a bolometer is effectively looking at a particular point for 1/4 of the time. Since the array is undersampled, the telescope secondary mirror is 'jiggled' to fill in the image; the polarization maps are usually sampled every 6″ but smoothed to about beam width spacing to improve σ_p. For an extended source, smoothing with e.g. a Gaussian function includes more flux and hence reduces t to obtain a given σ_p.

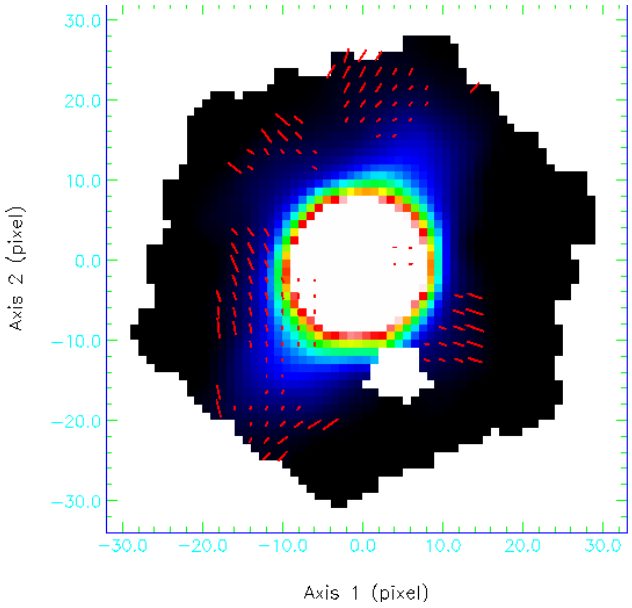

Figure 3. Typical 850 μm map of polarization measured around Jupiter, due to sidelobe IP. Vectors shown range from 0.8% to 15% (with criteria $p/\delta p > 2$ and $\delta p < 3\%$) and are plotted every $6''$ (2 pixels). Main-beam instrumental polarization has been subtracted. Data are from January 2000, using a 180 arcsec chop of the secondary mirror in the azimuth direction.

the alt-az telescope mounting and the fact that SCUBA is aligned with the elevation axis but is fixed on the Nasmyth platform. This angle relation is quite reliable, with deviations of around $\pm 15^\circ$ at extreme elevations, for the 850 μm pixels at the array edges that are furthest from the optical axis.

3.2 Sidelobe polarization

The sidelobes of the telescope beam have low intensity-amplitudes (e.g. $< 1\%$ at 850 μm at $> 40''$ from Jupiter in Figure 3), but different reflection and scattering effects for the two incoming planes of polarization can still produce instrumental 'sidelobe polarization'. This needs to be considered when observing extended sources, or faint objects next to much brighter ones, as the sidelobe IP can be considerable, and is additional to the main-lobe IP that has been measured using a compact planet.

In theory, a polarization map of an extended unpolarized source (generally Jupiter), made with the same primary dish surface and secondary mirror chop throw as the source observations, can be used for an exact subtraction of sidelobe IP. An example of such a map is shown in Figure 3, after subtraction of the standard main-lobe instrumental polarization. However, in practice it is often easier simply to estimate the error induced by the sidelobe effects. The most extreme case is seen with large chop throws of the secondary mirror (the maximum reccomended is $\pm 180''$) in a non-azimuthal direction. In this case, there are residual vectors towards about half of Jupiter's disk, with magnitudes up to 3%, although when *averaging* over this area (diameter of 40 arcsec) the net effect is only 0.25%. For smaller or azimuthal chop throws, the net residual is similar or lower and only about 1 in 10 individual points has a significant vector. Thus if the observer is interested in average polarization of an extended source, the error is quite small, but more careful calculations are required for data on a single map point in an extended region.

Additional problems arise if trying to extract source polarization when there is a much brighter object nearby in the field. In Figure 3, there are vectors averaging $\sim 6\%$ around Jupiter, although the largest tend to be at large radii where the power in the beam is low. A good general method is to set a threshold of *source* polarization percentage, above which sidelobe IP is not a serious contaminant, and to base this threshold on the relative polarized flux contributions. For example, if the instrumental polarized flux is half that of the source polarized flux, then in the worst case the two effects have orthogonal Stokes parameters, and the error in θ for the source will be $1/2 \tan^{-1} 0.5$ or only 13°. (If the effects are parallel, then the error will instead be in p, which is generally of less scientific importance.)

Taking into account the beam power profile, this criterion for the minimum believable source polarization percentage can be written

$$p_{crit} \geqslant 2 \times p_{sl} P_{sl} (F_{sl}/F) \quad (3)$$

where the three terms on the right-hand side are the IP at the relevant point in the sidelobe, the power here relative to the main beam, and the ratio of the flux of the object in the sidelobe to the flux in the main lobe. Thus sidelobe polarization can often be non-critical if the first two terms are small, even if there is a bright object in the sidelobe ($F_{sl} >> F$). As a quantitative example, Greaves (2002) observed polarization in the jets of the proto-planetary nebula CR 2688, at positions offset $15''$ from the central star. The ratio F_{sl}/F was 3.6, the average p_{sl} was 3% and the power at the edge of the main beam was $P_{sl} \approx 0.06$. Using Equation 3, the polarization of the southern jet was found to be believable because the measured value of 1.9% exceeded p_{crit} evaluated at 1.3%. At larger offsets, the critical product of power and IP tends to be smaller: for example the values < 0.01 and $\leqslant 15\%$ (Figure 3) give a smaller product than in the CRL 2688 case. The most critical quantity in individual sources is thus the flux ratio: very high contrasts will mean that faint regions need to be highly polarized to give usable results.

4 OBSERVING TECHNIQUES AND DATA REDUCTION

Data acquisition and reduction are based on extensions to standard techniques used at the JCMT; more details of the standard procedures are given in Holland et al. (1998, 1999), Jenness & Lightfoot (1998) and Jenness et al. (2000). For polarimetry, standard imaging or photometry observations are made at a set of waveplate positions (normally 0, 22.5, 45, 67.5, 90... 337.5°), and these data are fitted to detect the sinusoidal signal modulation from rotating the incoming polarization vector. Using a complete cycle is intended to eliminate other modulations such as reflections off the waveplate. An alternative to fitting is direct subtraction of data taken at different angles, as for example, $p\ cos(2\theta)$ can be found from $(S(45) - S(0))/(S(45) + S(0))$ and $p\ sin(2\theta)$ from $(S(67.5) - S(22.5))/(S(67.5) + S(22.5))$ (Equation 1); this method is entirely valid and gives both Stokes parameters directly, but is less often used. For an excellent introduction to polarization observing procedures and limitations, see also Hildebrand et al. (2000).

4.1 Observing modes

Three observing modes have been adapted for use with the polarimeter. These are *photometry*, where a single bolometer observes a fixed point; *jiggle-mapping*, where the secondary mirror is jiggled to obtain an image of one SCUBA field-of-view, using all

the bolometers in an array; and *scan-mapping*, where the telescope scans across a source and the data from all bolometers are reconstructed to give large images. All of these modes use chopping of the secondary mirror to remove the sky emission; photometry and jiggle-mapping also nod the source between left and right beams halfway through an observation to minimise sky gradients. For polarimetry, the only difference is that a complete standard observation is made at each waveplate angle before moving on to the next angle.

The first two polarimetry modes are fully commissioned, and the third has been proven experimentally but is not yet fully integrated. All six of the available SCUBA wavelengths have been used, but only a small number of observations have been made with the 350/750 μm filter combination or using the 2 mm photometric pixel (less than 1% each of the total number of observations). Thus the best quantified performance is at 850 and 1350 μm; 450 μm data are obtained simultaneously with 850 μm but are often not usable due to poor atmospheric transmission. Scan-mapping has been tested only at 850 μm.

The photometry mode is most suited to sources with accurately known positions that are smaller than the telescope beam width (8, 15 and 24 arcsec at 450, 850 and 1350 μm). The off-source bolometers remain 'switched-on' and can be used to subtract residual sky signals (not possible with the individual photometric pixels at 1350 and 2000 μm). Typically the secondary mirror chops between on- and off-source with a 1 arcmin throw, to allow subtraction of the sky DC-level, and 8 seconds of data are obtained at each of the 16 waveplate positions. The chop takes place at a rate of 7.8 Hz, and the telescope nods so that the source moves from the left beam to the right beam after 4 seconds. A small grid of points can be used rather than a fixed point but this in not generally done. Integrations of up to about 20 seconds can provide higher signal-to-noise in stable conditions, but generally many short integrations are co-added.

The jiggle map mode is typically used for sources bigger than the beam but smaller than the 2.3 arcmin array field-of-view in at least one dimension. If the source is larger, two effects can corrupt the polarization measurement (Matthews et al. 2001). Firstly, the maximum recommended chop throw is 3 arcmin, so sources larger than this will be 'self-chopped'. In practice sky noise subtraction requires several emission-free bolometers, so the setting of the zero level will be inaccurate if the source dimensions approach 3 arcmin; an incorrect zero-level changes I_u and so alters the percentage polarization. Secondly, if there is emission in the reference, i.e. nominally off-source, beams it may well be polarized and this can corrupt the on-source polarized signal in both magnitude and direction. A limit can be estimated where the reference polarization is not known, but this may not set useful constraints: for example, faint outer regions in some dust clouds can be up to $\sim 15\%$ polarized (e.g., Matthews et al. 2001).

A 16-point jiggle sequence with the secondary mirror gives an 850 (or 750) μm image with a point every 6 arcsec, so is slightly better than Nyquist (half-beam) sampled. The simultaneous data at 450 (or 350) μm are undersampled, since the points are only a little better than a beam width apart, and a 64-point jiggle sequence with 3 arcsec sampling is required if these data are of importance. The simpler jiggle takes 32 seconds to complete at each waveplate position, and the more complete jiggle takes 128 seconds, so the former is preferable for greater sky stability.

The scan map mode has been tested at 850 μm only, on a few sources with sizes of about 6–10 arcmin. The technique used is to scan the telescope across the source in any suitable direction, while chopping in RA or Dec. Using two different chop throws in each direction, for a total set of four, has been found to give good reconstructed images; further details of this 'Emerson II' technique are given by Jenness et al. (2000). It is important to scan off-source so that a true baseline can be established and set to zero in each individual waveplate image, before the polarization reduction is done.

The scan rate used is 48 arcsec per second, so sampling every 1/8th second gives points 6 arcsec apart, the same as in jiggle mapping. The minimum number of waveplate positions needed to deduce the Stokes parameters is four, so scan map polarimetry is rather time-consuming, for example, taking 30 minutes for one dataset on a 400 arcsec square area. This compares to three minutes or less for a set of Stokes parameters in the other modes, so scan map polarization measurements require more stable conditions.

4.2 Data reduction techniques

Two separate software packages are used for the data reduction: one for photometric polarimetry (SIT: Nartallo 1995) and one for imaging polarimetry (POLPACK: Berry & Gledhill 2000). The reduction philosophy is the same in both cases, and in fact POLPACK can handle single-pixel 'images', while SIT is more optimised for inspecting the results of individual waveplate cycles on a single point.

The raw data are reduced (Jenness et al. 2002) by extracting the chopped signals, flatfielding, and correcting for atmospheric extinction using a skydip. This is a series of measurements of sky emission at different elevations, made either with the JCMT at the observing wavelength, or taken from the 1.3mm database recorded at the adjacent Caltech Submillimeter Observatory (CSO) and extrapolated in wavelength. The next refinement is to subtract rapid changes in sky emission (to a greater accuracy than achieved simply by chopping: (Holland et al. 1999)) by shifting the mean level using blank bolometers in the array, or in scan-mapping, subtracting smoothed data seen by each bolometer over 2 seconds. This 'sky noise' is spatially correlated over the array diameter (Jenness, Lightfoot & Holland 1998).

The main lobe instrumental polarization is then removed on a bolometer-by-bolometer basis using the expression:

$$S_{corrected} \approx \frac{S_{measured}}{1 + p_{IP}(e)\cos(4\delta - 2\theta_{IP}(e))} \quad (4)$$

where $p_{IP}(e), \theta_{IP}(e)$ are the percentage and direction of instrumental polarisation at elevation e (a constant percentage is generally assumed). This is an approximation of

$$S_{corrected} = S_{measured} - S_{mean} p_{IP}(e)\cos(4\delta - 2\theta_{IP}(e)) \quad (5)$$

and is valid for instrumental polarizations of up to a few percent. The former expression is prefered as the mean flux level is not easily determined prior to regridding — the bolometer jiggles to different source positions and thus only part of the data stream refers to a particular spatial point. Also, not exactly the same point is seen by this bolometer for the next waveplate angle, because of sky rotation (SCUBA does not use an image de-rotator).

In imaging mode the data are then regridded to a rectangular array, removing pixels from the edge that are affected by regridding edge effects in order to simplify mosaicing. For scan map data, a Fourier deconvolution is used to remove the chop signature and combine the four different chopped maps (Jenness et al. 2000).

The Stokes parameters I, Q, U are then extracted by fitting the signal in each pixel as a function of waveplate angle; errors

are supplied by comparing signals at identical or equivalent waveplate positions (e.g. 0, 90, 180 and 270°; see Eq. 1[4]) In SIT, the Q and U are then listed and statistical tests can be used to reject anomalous fits before calculating averages and deducing p, θ. In POLPACK, an I, Q, U data-cube is generated and a catalogue of vectors produced corresponding to all the image pixels. When combining different data sets (a set contains 16 waveplate positions) it was determined that the best results were obtained by coadding the IQU cubes rather than adding more data to the fit. As more data were added to the fit the signal-to-noise did not increase in the expected way, suggesting that it was susceptible to DC-level differences amongst the observations.

Various binning and selection procedures can be used to improve the polarization signal-to-noise. Typical criteria are $p/\delta p > 3$ (i.e. $\delta\theta < 10^\circ$) and an upper limit such as $\delta p < 1 - 2\%$ to eliminate biased data. Because the waveplate angles increase step by step, a linear drift in the sky transmission can force, for example, a positive Q and U, and these spurious fits tend to produce a high p, especially in regions of low I. Thus a δp criterion can eliminate such data with a large scatter between good and inaccurate fits. For example, four measurements with similar θ but $p = 3, 3, 3, 9\%$ would give an average p of 4.5% and a standard error of 1.3% (hence $p/\delta p = 3.5$). This dataset is clearly biased by the last measurement, but could be eliminated with a $\delta p < 1\%$ criterion. This entire reduction process has been automated using the ORAC-DR data reduction pipeline (Economou et al. 1998; Jenness & Economou 1999).

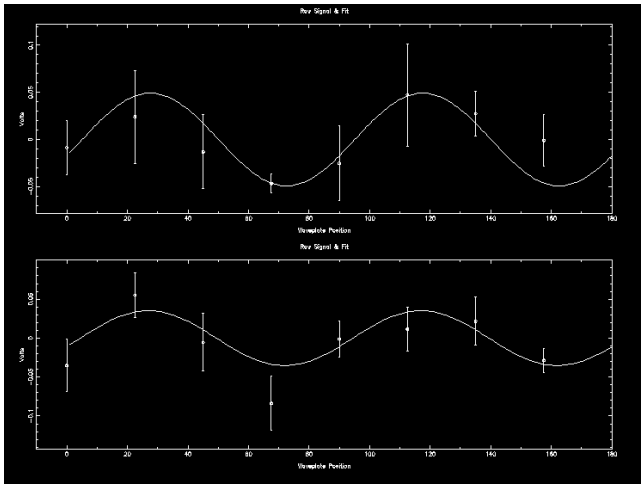

Figure 4. Fits to 2000 μm photometric polarimetry of Sgr A*, illustrating data quality for one waveplate cycle on an 8 Jy, 3% polarized source (instrumental polarization of 1.4% has not yet been subtracted). The axes are measured signal modulation versus waveplate orientation, and the scales are polarization fraction (tick marks at intervals of 0.01, i.e. 1%) versus angle (tick marks at 10° intervals). The top plot covers $\delta = 0^\circ - 157.5^\circ$ and the bottom plot is for $\delta = 180^\circ - 337.5^\circ$. Good consistency is demonstrated by the upper and lower fits from the first and second halves of the waveplate cycle being in phase.

5 SCIENTIFIC CAPABILITY

Science targets so far observed include asteroids, planetary nebulae, supernova remnants, T Tauri star disks, accreting protostars, pre-stellar cores, Bok globules, dark cloud filaments, high-mass star-forming clouds, the Galactic Centre including the black hole Sgr A*, the starburst galaxy M82, the ultraluminous galaxy Arp 220 and a number of variable AGN or 'blazars'. Results have been discussed by Tamura et al. (1999); Matthews & Wilson (2002); Davis et al. (2000); Ward-Thompson et al. (2000); Henning et al. (2001); Vallée et al. (2000); Feldman et al. (2000); Aitken et al. (2000); Greaves et al. (2000); Marscher et al. (1999), among others. Many of these objects have sub-Jy fluxes per beam, and were not feasible to observe before SCUBA; they are also very difficult for other ground-based instruments such as the HERTZ polarimeter-camera used at the CSO, which operates in the more challenging 350 μm band (Dowell et al. 1998). Examples of some typical observations are described below; the imaging results shown in the figures have not previously been published.

5.1 Polarimetric Photometry

Sgr A*, the massive black hole candidate at the centre of the Galaxy, was observed polarimetrically by Aitken et al. (2000). Crucial observations were made at 1350 and 2000 μm in the photometric mode, to establish the polarization spectrum in the millimetre regime as well as at submillimetre wavelengths. These were the first detections of linear polarization of Sgr A*, and they showed a dramatic $\sim 90^\circ$ shift in position angle around 1 mm wavelength, which implies self-absorption in a very compact emission region of only a few Schwarzschild radii (Aitken et al. 2000; Bromley et al. 2001; Liu & Melia 2002). The 1350 and 2000 μm detections were each significant at the 10 sigma level after about 15 minutes of integration. An example of the fitted results from one waveplate cycle (2 minutes of data) is shown in Figure 4.

It is now routinely possible to detect polarized emission from compact radio sources. A $\sim 5\sigma$ detection of a 0.5–10 Jy source can be made in 30–60 minutes, depending on the fractional polarization (values of 2–40% have been observed). Large levels of polarization indicate that the magnetic field must be quite highly ordered, and allow its direction to be inferred without worrying about opacity effects. Comparisons with quasi-simultaneous results from 7 mm very long base line interferometry show that, in many cases, the angle of submillimetre polarization matches that very close to the base of the sub parsec-scale jet, and/or the structural position angle of the jet (Stevens et al. in prep.).

One of the faintest photometric detections with the UKT14 polarimeter was the HH24MMS protostar observed by Greaves, Holland & Ward-Thompson (1997) at 800 μm. This result was confirmed with the SCUBA polarimeter at 850 μm: HH24MMS was 3.7 ± 1.3% polarized at 95 ± 10° in the earlier data and the new measurement was 3.82 ± 0.61% at 109 ± 5°. Thus results published with the old instrument appear to be quite reliable, but now much fainter targets can be detected.

5.2 Polarimetric Imaging of Single Fields

Jiggle map polarimetry has been used for a wide variety of targets: Figure 5 illustrates results for the high-mass star-formation region W3. The two bright cores contain the luminous clusters of young stellar objects IRS5 and IRS4 (left and right respectively), plus an extended envelope. The image illustrates the care that must

[4] Scan map observations are sufficiently time-consuming that only the angles $\delta = 0, 22.5, 45, 67.5^\circ$ may be used, in which case the same angle in different cycles should be compared.

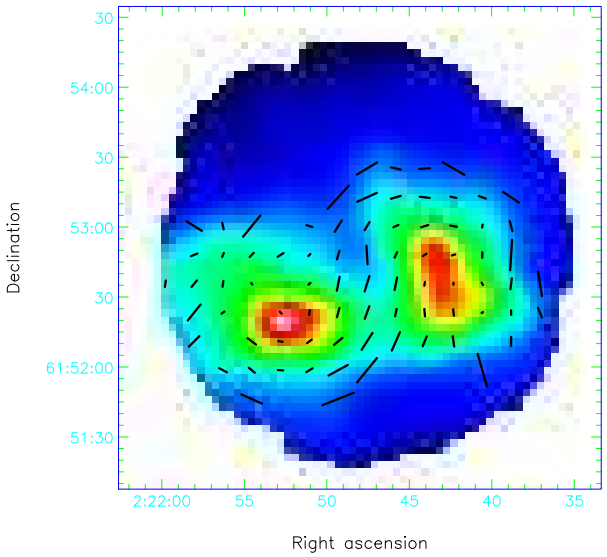

Figure 5. 850 μm polarization map of the main cores in W3 (see text). The colour scale goes up to 8 Jy/beam and the vectors range from 0.4% to 7.6%; co-ordinates are B1950. All detections have $p/\delta p > 3$ and $\delta p < 1\%$. The E-plane of polarization is plotted, i.e. parallel to the long axes of aligned dust grains and perpendicular to the aligning magnetic field.

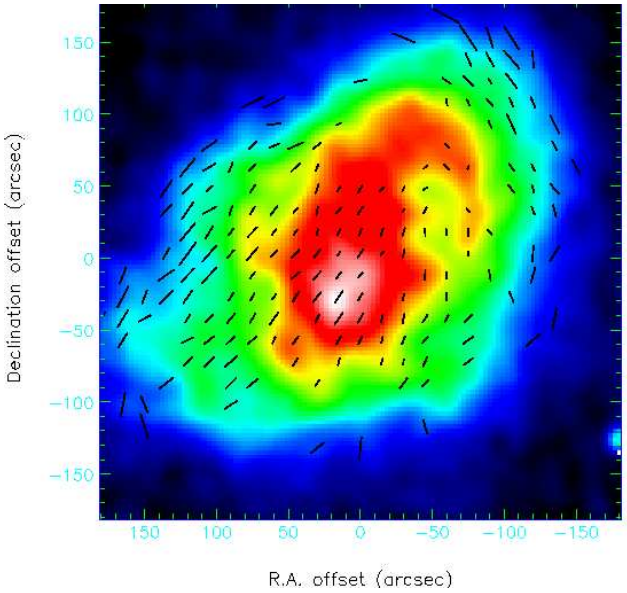

Figure 6. 850 μm polarization data for the Crab Nebula, using scan map polarimetry. The smallest and largest polarization vectors are 8% and 58%, and the colour scale goes up to 1.8 Jy/beam at 850 μm. There are 183 vectors with $p/\delta p > 5$, at beam width spacing, after 1 hour of integration.

be taken to chop in the direction of the faintest extended emission (here at a position angle of 20° east-of-north and 2.5′ throw); there are some minor discrepancies with the 350μm polarization map of Schleuning et al. (2000), which can plausibly be explained by their larger (and more suitable) 6.3′ chop throw. Examination of a JCMT archival 850 μm scan-map shows that the faintest regions with plotted vectors in Figure 5 have in the worst cases up to 25% relative flux in one of the off-beams. Although no large-scale polarization data are available, we can estimate that a 10% polarization at this off-point would seriously contaminate a 2.5% on-source vector.

Projects on regions such as W3 are producing very valuable information on different magnetic morphologies in clouds with more or less active star formation and varying core and star masses (Matthews & Wilson 2002, 2000; Coppin et al. 2000; Davis et al. 2000; Fiege & Pudritz 2000). Also, the marked decrease in polarization with increasing flux can be used to test models of field lines that are tangled or turbulent within the beam, and/or models of grains that are less well aligned in dense cores (Ostriker et al. 2001; Arce et al. 1998).

The faintest targets detected with jiggle map polarimetry have fluxes of about 0.2 Jy/beam and a few percent polarization. This covers a wide range of Galactic interstellar clouds and also the closest star-forming galaxies (Greaves et al. 2000). Observing efficiency compared to previous point-by-point magnetic field mapping has been greatly increased: for example, the 800μm polarimetry of the W3-IRS4 core reported by Greaves et al. (1999) required one hour of observation per spatial point, whereas the data in Figure 5 took a similar time for 78 detected points going down to much lower flux limits.

5.3 Polarimetric Scan-mapping

Scan map polarimetry is still under development, but initial tests on the polarized synchrotron emission of the Crab Nebula gave very good results (Figure 6). The 850 μm polarization was very similar between scan map observations and a standard jiggle map (of the central 3 arcmin); percentages and angles differed by only 1% and 6° (the latter is probably dominated by rotation of a few degrees during each 30 minute map sequence). The angles also agree very well with 9 mm results published by Flett & Henderson (1979). However, the SCUBA data improve our understanding of the (sub)millimetre polarization pattern from 90 to 15 arcsecond resolution, greatly clarifying the geometry around features such as the emission 'arm' to the north-west. The average flux and polarization for the Crab Nebula are 1 Jy/beam and 25%, and $\geqslant 5\sigma$ detections were obtained in one hour of observing. A more typical source with an equivalent polarized flux, such as a 5 Jy/beam, 5% polarized dust cloud, should be detectable in the same time.

6 CURRENT AND FUTURE DEVELOPMENTS

Work is ongoing on automating scan-map polarimetry and expanding the use of 450 μm polarimetry. The latter will give a factor of two improvement in spatial resolution over 850 μm but not all the IP data have been obtained. Fast corrections for atmospheric changes are also being tested, utilising a water vapour radiometer (Wiedner et al. 2001) in the JCMT's receiver cabin. This monitors the profile of the 183 GHz atmospheric absorption line about every second, and thus gives a very precise transmission measurement along the same line-of-sight as the source. Some tests have also been made of a 'continuous spinning' mode, as an alternative to stepping the waveplate to discrete angles. By analysing the power spectrum of the signal, it is possible to detect the intensity of the polarized signal (a modulation every 90°), and the position angle can also be measured by retaining information on orientation as a function of time. This should be a very fast method of detecting strong sources, and rapid spinning (e.g. > 1 Hz) would eliminate most problems with the sky changing before the complete polarized modulation has been detected.

Finally, a replacement camera is currently being built by the

UK Astronomy Technology Centre. With SCUBA-2 and a new polarimeter, there should be a factor of 2.5 decrease in NEFD, a factor of 16 increase in imaging speed due to instantaneous full-sampling (no jiggling) and a 15-fold increase in field-of-view, combining to give an improvement in polarization imaging power for large sources of ~ 1500.

7 SUMMARY

An efficient polarimeter coupled with a very sensitive submillimetre camera has facilitated a major advance in ground-based imaging polarimetry. The variety of science targets has also expanded, with almost every category of Galactic source of dust and synchrotron emission becoming available, as well as a number of extragalactic objects. Investigations of the dust polarization spectrum can also be made, especially in conjunction with 60–350 μm polarization data from the Kuiper Airborne Observatory and the CSO (Hildebrand et al. 2000; Dotson et al. 2000). This reveals unique information about the relation of grain alignability and emissivity, particularly in mixed grain populations (Greaves et al. 1999; Hildebrand et al. 1999). Finally the multi-wavelength capability of the SCUBA Polarimeter covers both the high-frequency end of synchrotron spectra and the long-wavelength tail of dust spectra, where both effects are generally optically thin and easiest to interpret.

ACKNOWLEDGEMENTS

The JCMT is operated by the Joint Astronomy Centre on behalf of PPARC of the UK, the Netherlands OSR, and NRC Canada. We acknowledge the software and support provided by the Starlink Project which is run by CCLRC on behalf of PPARC. We especially wish to thank the many members of JCMT staff involved in commissioning and maintaining the SCUBA Polarimeter.

REFERENCES

Aitken D. K., Greaves J., Chrysostomou A., Jenness T., Holland W., Hough J. H., Pierce-Price D., Richer J., 2000, ApJ, 534, L173

Arce H. G., Goodman A. A., Bastien P., Manset N., Sumner M., 1998, ApJ, 499, L93

Berry D. S., Gledhill T. M., 2000, POLPACK. Starlink User Note 223, Starlink Project, CLRC

Bromley B. C., Melia F., Liu S., 2001, ApJ, 555, L83

Clemens D. P., Kane B. D., Leach R. W., Barvainis R., 1990, PASP, 102, 1064

Coppin K. E. K., Greaves J. S., Jenness T., Holland W. S., 2000, A&A, 356, 1031

Davis C. J., Chrysostomou A., Matthews H. E., Jenness T., Ray T. P., 2000, ApJ, 530, L115

Dotson J. L., Davidson J., Dowell C. D., Schleuning D. A., Hildebrand R. H., 2000, ApJS, 128, 335

Dowell C. D., Hildebrand R. H., Schleuning D. A., Vaillancourt J. E., Dotson J. L., Novak G., Renbarger T., Houde M., 1998, ApJ, 504, 588+

Economou F., Bridger A., Wright G. S., Rees N. P., Jenness T., 1998, in ASP Conf. Ser. 145: Astronomical Data Analysis Software and Systems VII. pp 196+

Feldman P. A., Redman R. O., Carey S. J., Egan M. P., 2000, in American Astronomical Society Meeting. pp 0514+

Fiege J. D., Pudritz R. E., 2000, ApJ, 544, 830

Flett A. M., Henderson C., 1979, MNRAS, 189, 867

Flett A. M., Murray A. G., 1991, MNRAS, 249, 4P

Glenn J., Walker C. K., Young E. T., 1999, ApJ, 511, 812

Greaves J. S., 2002, A&A, in press

Greaves J. S., Holland W. S., Jenness T., Hawarden T. G., 2000, Nature, 404, 732

Greaves J. S., Holland W. S., Minchin N. R., Murray A. G., Stevens J. A., 1999, A&A, 344, 668

Greaves J. S., Holland W. S., Ward-Thompson D., 1997, ApJ, 480, 255+

Henning T., Wolf S., Launhardt R., Waters R., 2001, ApJ, 561, 871

Hildebrand R. H., Davidson J. A., Dotson J. L., Dowell C. D., Novak G., Vaillancourt J. E., 2000, PASP, 112, 1215

Hildebrand R. H., Dotson J. L., Dowell C. D., Schleuning D. A., Vaillancourt J. E., 1999, ApJ, 516, 834

Holland W. S., Cunningham C. R., Gear W. K., Jenness T., Laidlaw K., Lightfoot J. F., Robson E. I., 1998, in Proc. SPIE Vol. 3357, p. 305-318, Advanced Technology MMW, Radio, and Terahertz Telescopes, Thomas G. Phillips; Ed.. pp 305–318

Holland W. S., Robson E. I., Gear W. K., Cunningham C. R., Lightfoot J. F., Jenness T., Ivison R. J., Stevens J. A., Ade P. A. R., Griffin M. J., Duncan W. D., Murphy J. A., Naylor D. A., 1999, MNRAS, 303, 659

Jenness T., Economou F., 1999, in Mehringer D. M., Plante R. L., Roberts D. A., eds, ASP Conf. Ser. Vol. 172, Astronomical Data Analysis Software and Systems VIII. Astron. Soc. Pac., San Francisco, p. 171

Jenness T., Holland W. S., Chapin E., Lightfoot J. F., Duncan W. D., 2000, in ASP Conf. Ser. 216: Astronomical Data Analysis Software and Systems IX. pp 559+

Jenness T., Lightfoot J. F., 1998, in Albrecht R., Hook R. N., Bushouse H. A., eds, ASP Conf. Ser. Vol. 145, Astronomical Data Analysis Software and Systems VII. Astron. Soc. Pac., San Francisco, p. 216

Jenness T., Lightfoot J. F., Holland W. S., 1998, Proc. SPIE, 3357, 548

Jenness T., Lightfoot J. F., Holland W. S., Greaves J. S., Economou F., 2000, in ASP Conf. Ser. 217: Imaging at Radio through Submillimeter Wavelengths. pp 205+

Jenness T., Stevens J., Archibald E. N., Economou F., Jessop N. E., Robson E. I., 2002, MNRAS, 336, 14

Kane B. D., Clemens D. P., Barvainis R., Leach R. W., 1993, ApJ, 411, 708

Liu S., Melia F., 2002, ApJ, 573, L23

Marscher A. P., Marchenko S. G., Stevens J. A., Gear W. K., Lister M. L., Cawthorne T. V., Stirling A., Gómez J. L., Gabuzda D. C., Robson E. I., 1999, in American Astronomical Society Meeting. pp 8902+

Matthews B. C., Wilson C. D., 2000, ApJ, 531, 868

Matthews B. C., Wilson C. D., 2002, ApJ, 574, 822

Matthews B. C., Wilson C. D., Fiege J. D., 2001, ApJ, 562, 400

Murray A. G., Nartallo R., Haynes C. V., Gannaway F., Ade P. A. R., 1997, in The Far Infrared and Submillimetre Universe.. pp 405+

Naghizadeh-Khouei J., Clarke D., 1993, A&A, 274, 968+

Nartallo R., 1995, Ph.D. Thesis, pp 54+

Nartallo R., Gear W. K., Murray A. G., Robson E. I., Hough J. H., 1998, MNRAS, 297, 667

Novak G., Gonatas D. P., Hildebrand R. H., Platt S. R., Dragovan M., 1989, ApJ, 345, 802

Ostriker E. C., Stone J. M., Gammie C. F., 2001, ApJ, 546, 980
Schleuning D. A., 1998, ApJ, 493, 811+
Schleuning D. A., Vaillancourt J. E., Hildebrand R. H., Dowell C. D., Novak G., Dotson J. L., Davidson J. A., 2000, ApJ, 535, 913
Tamura M., Hough J. H., Greaves J. S., Morino J., Chrysostomou A., Holland W. S., Momose M., 1999, ApJ, 525, 832
Title A. M., Rosenberg W. J., 1981, in Proc. SPIE Vol. 307, p. 120+, Polarizers and Applications, G. B. Trapani; Ed.. pp 120+
Vallée J. P., Bastien P., Greaves J. S., 2000, ApJ, 542, 352
Ward-Thompson D., Kirk J. M., Crutcher R. M., Greaves J. S., Holland W. S., André P., 2000, ApJ, 537, L135
Wiedner M. C., Hills R. E., Carlstrom J. E., Lay O. P., 2001, ApJ, 553, 1036

This paper has been typeset from a TEX/ LATEX file prepared by the author.